12,05

Studies of magnetic nanoparticles $Mn_xFe_{3-x}O_4$@OA ($0 \leq x \leq 1.0$) functionalized with oleic acid (OA) for biomedical applications

© A.S. Kamzin[1], N. Dogan[2,3], O.M. Dogan[2], V.G. Semenov[4]

[1] Ioffe Institute,
St. Petersburg, Russia
[2] Department of Physics, Gebze Technical University,
41400 Kocaeli, Turkey
[3] Department of Physics Engineering, Faculty of Science and Letters, Istanbul Technical University,
34469, Istanbul, Turkey
[4] St. Petersburg State University,
St. Petersburg, Russia

E-mail: ASKam@mail.ioffe.ru

Received June 28, 2023
Revised June 28, 2023
Accepted June 30, 2023

Functionalization of magnetic nanoparticles (MNP) is a unique of magnetic nanoparticles (MNP) is a unique tool for creating particles with the properties required for biomedical applications. Therefore, the study of the magnetic properties of coated MNPs is the most important task of our time. The effect of changes in the concentration of Mn ions on the properties of $Mn_xFe_{3-x}O_4$ nanoparticles coated with oleic acid (OA) $Mn_xFe_{3-x}O_4$@OA (where $x = 0$, 0.25, 0.5, 0.75 and 1.0) to create stabilized magnetic fluids for various applications is investigated. The synthesis of $Mn_xFe_{3-x}O_4$@OA MNPs was carried out by thermal decomposition using manganese-oleate and iron oleate. The properties and phase states of the obtained MNPs were studied by X-ray diffraction (XRD) and Mössbauer spectroscopy. To understand the behavior of MNPs in small magnetic fields during hyperthermic treatment, Mössbauer studies of $Mn_xFe_{3-x}O_4$@OA particles were carried out when a magnetic field with a strength of 1.7 kOe was applied. It is established that the thermal decomposition method makes it possible to obtain single-phase superparamagnetic particles promising for biomedical applications

Keywords: magnetic nanoparticles (MNP) $Mn_xFe_{3-x}O_4$, MNP fuctionalised by oleic acid $Mn_xFe_{3-x}O_4$@OA, magnetic properties, structure, Mössbauer spectroscopy.

DOI: 10.61011/PSS.2023.08.56587.127

1. Introduction

Magnetic nanoparticles (MNPs) of diameter from 1 to 100 nm have properties significantly different from those of macroscopic crystals, namely, superparamagnetism, increased anisotropy of the surface layer, a significant increase in coercive force, high thermal stability, catalytic activity, etc. Therefore, at present, one of the main issues of fundamental physics of magnetism is the study of such a variety of properties of MNPs. On the practical side, variations of technological techniques make it possible to create magnetic nanoparticles with the required parameters for a variety of applications, the most important of which is biomedicine: cell separation, genetic engineering and therapy, contrast enhancement in magnetic resonance imaging, magnetic diagnostic systems of molecular imaging, biosensors, magnetic powder, targeted drug delivery and magnetic hyperthermia for cancer treatment [1–3]. However, direct administration of MNPs into the body is impossible, since they can be identified by the immune system as foreign particles toxic to the human body and destroyed [4,5]. MNPs are encapsulated in a non-toxic non-magnetic material for biomedical applications. Thus, particles of hexagonal barium ferrite ($BaFe_{12}O_{19}$), which has high magnetic characteristics compared to magnetite or maghemite, [4], used for local hyperthermia treatment of cancerous tumors (see [5] and references there), were encapsulated in biologically compatible hydroxyapatite [4]. MNP is delivered to the tumor tissues for the hyperthermia treatment of cancerous tumors and is exposed to an alternating radiofrequency magnetic field, the energy of which is converted into thermal energy due to relaxation mechanisms. This leads to heating of the MNPs and, accordingly, the tumor tissues where the MNPs are located and necrosis of malignant cells occurs at temperatures of 44−45°, which are more sensitive to temperature than healthy tissues [1].

Various applications of MNPs, including in biomedicine, are possible with the use of ferrofluids (FF) or liquids with nanoparticles, first obtained in the 1960s (see [6] and references there). Ferrofluids are highly stable colloidal magnetically controlled suspensions consisting of MNPs dispersed in appropriate carrier liquids and suspended in it [7–9], being in fact an achievement of the science of colloids. The FFs should be stable and should not delaminate when a magnetic field is applied, and after it is turned off, the FFs should recover their original characteristics,

which allows manipulating and controlling the FF. The main component of FFs are magnetic nanoparticles, the weight content of which can reach 25%. MNP stability is achieved by treatment with surfactants (surfactants), chemical compounds adsorbed by the surface layer of MNP and causing a decrease in surface tension [10–15]. The stabilization of particles simplifies the functionalization, that is, the attachment of therapeutic (medicinal) drugs to them. Extensive studies in the last decade have been directly related to the creation of MNPs for specific applications and are aimed at: a) the development of methods for the synthesis of single-phase homogeneous particles of a given shape, size and size distribution that determine the magnetic properties of MNPs [3]; b) the creation of safe MNPs with high colloidal stability in biological environments [16,17]; c) creation of multifunctional structures for theranostic applications [16]. The treatment of malignant tumors using FF attracts a lot of attention of researchers because of such advantages as the possibility of guided and localized therapy, etc., [18].

The requirement for the MNPs used in biomedicine was the stabilization of particles and the functionalization of their surface using surfactants such as citric or oleic acid (OA), polymers (polyethylene glycol), polylactic-co-glycolic, polyacrylic and other acids, natural dispersants (chitosan, dextran, gelatin, starch, albumin, liposomes, etc.) [10–17,19–22].

The choice of magnetic materials is quite wide, but for the creation of colloidal suspensions with the necessary stability, an important factor is the good compatibility of nanoparticles with a surfactant and a carrier liquid, which significantly reduces this choice. Magnetite (Fe_3O_4) and maghemite ($\gamma-Fe_2O_3$) [18,21–23], whose magnetic parameters currently do not meet the requirements of bimedicine are biologically compatible and widely used in biomedicine. Ferrites-spinels of the type MFe_2O_4, have high magnetic characteristics, and without loss of biocompatibility inherent in iron oxides [1–3,15,21,23] and $M_x^{2+}Fe_{3-x}^{3+}O_4^{2-}$ [17,18,22–30] and where $M = Mn^{2+}$, Zn^{2+}, Co^{2+}, Mg^{2+}, Ni^{2+} and others. Lower toxicity, low saturation magnetization values, high corrosion resistance, magnetocrystalline anisotropy and magnetic susceptibility, insignificant coercivity, as well as high stability and colloidal dispersibility in physiological fluids, make such MNPs promising for biomedicine [12,13].

The size and structure of the particles $M_x^{2+}Fe_{3-x}^{3+}O_4^{2-}$ significantly depend on the synthesis method and chemical composition. Methods such as pyrolysis, mechanical fusion, hydrothermal method, mechanochemical synthesis, plasma synthesis, thermal decomposition, co-deposition, mechanical grinding, sonochemical method, etc. [7–8,12–14,25] are used for the synthesis of MNPs, of which the methods of synthesis of thermal decomposition and co-deposition is the simplest, most reliable and allowing for obtaining more stable particles [12–14,30,31]. The source of the formation of magnetic properties of particles $M_x^{2+}Fe_{3-x}^{3+}O_4^{2-}$ are super-exchange interactions of tetrahedral cations (A) and octahedral [B] positions through oxygen ions. Therefore, it is possible to obtain particles $M_x^{2+}Fe_{3-x}^{3+}O_4^{2-}$ with the required electrical, optical and magnetic properties, such as magnetization, anisotropy, coercive and hyperfine fields by controlling the distribution of cations by (A) and [B] positions, selecting the chemical composition and type of cations.

The ions Mn [12,17,22,26,28,29–32] are attractive for doping (substitution of Fe^{2+} ions) in Fe_3O_4, their peculiar feature is the difference in the mechanisms of substitution of iron ions in nonequivalent sublattices in the structure Fe_3O_4. The magnetic properties of MNPs, including the value of Ms, significantly depend on the type of doped ions, on particle sizes, on the distribution of cations over sublattices, which allows synthesis technologies to control saturation magnetization (Ms) and the coercive force of particles and obtain superparamagnetic particles $Mn_xFe_{3-x}O_4$ [12,17,28,30–32], having the highest heating rate by a magnetic field [13]. Consequently, the material and thickness of the coating are the determining factors in explaining the differences that arise during the functionalization of MNPs, and this requires systematic study of functionalized MNPs. This paper presents the results of studies of the properties of thermal decomposition of magnetite nanoparticles synthesized by metol, doped with Mn ions ($Mn_xFe_{3-x}O_4$ at $x = 0$, 0.25, 0.5, 0.75, 1.0) coated with oleic acid (OA) ($Mn_xFe_{3-x}O_4$@OA). The magnetic structure of the particle determines the magnetic characteristics of nanoparticles, therefore, the analysis of the formation of the magnetic structure of the MNP $Mn_xFe_{3-x}O_4$@OA was conducted. Mössbauer studies of MNP $Mn_xFe_{3-x}O_4$@OA were carried out when applying weak magnetic fields used in hyperthermia to understand the mechanisms of the influence of magnetic hyperthermia on the properties of particles.

2. Experimental part

The thermal decomposition method is chosen for the synthesis of MNP $Mn_xFe_{3-x}O_4$, which is the most promising because of its simplicity, performance and control of a number of factors, such as size, morphology, composition and degree of agglomeration, by changing the conditions experiment (temperature, time, reagents and mixing rate) [12–14,30,31].

The nucleation of particles in the thermal decomposition method occurs when a metal precursor is added to a heated solution in the presence of surfactants. An increase in the reaction temperature leads to the growth of particles, and the composition and size of the formed particles depend on the reaction time, temperature. In the case of iron oxide particles, the thermal decomposition of the precursor initially leads to the formation of iron MNPs, followed by their oxidation in air. The inevitability of oxidation under normal conditions requires control of the reaction path and, thereby, control the properties of the obtained MNPs. The

stages of nucleation and growth of particles are separated in this method, since they take place at different temperatures, which is an advantage compared to other methods.

Oleic acid (OA) was chosen as a stabilizing agent from the family of amphiphilic surfactants because of its electrostatic with biocompatible properties and low cost [10,12–15,19–21]. Moreover, OA makes it possible to control the growth of crystallites, since it stops the maturation process, provides steric stabilization of MNPs and prevents from agglomeration. The presence of oleic acid affects the magnetic properties of MNPs by changing the distances between the particles and, thus, their interaction. It is important that OA is not only harmless to a living organism, but it is also significantly useful, since without OA proper metabolism, the fight against cholesterol, and strengthening immunity are impossible.

2.1. Synthesis of nanoparticles $Mn_xFe_{3-x}O_4$@OA ($x = 0, 0.25, 0.5, 0.75, 1.0$)

The synthesis of MNP of magnetite (Fe_3O_4) doped with manganese $Mn_xFe_{3-x}O_4$, by thermal decomposition, unlike the traditional method of obtaining MNP of oxides iron coated with acids was carried out in two stages [12]. Fe-oleate and Mn-oleate complexes (precursors) were prepared at the first stage. 10 mmol of chloride hexahydrate, 30 mmol of oleic acid and methanol were mixed in a magnetic stirrer until dissolved in each other to obtain iron oleate. A mixture of methanol and 30 mmol sodium hydroxide was placed in a burette and dripped into the solution with magnetic stirring. Upon completion of the reaction, the red-brown Fe-oleate powder was separated, the solution was washed several times with methanol and then heated for 30 minutes in an oven at 55°C. The resulting iron oleate was mixed with the solvent used in the reaction. This mixing was performed in a magnetic stirrer at 70°C, controlling the addition of solvent to the mixture, and this process continued until a homogeneous solution was obtained. The red-brown structure of Fe-oleate was separated by washing the solution several times at the end of the reaction. Similarly, the Mn-oleate reaction was carried out by stirring with a magnetic stirrer at 70°C for 30 min.

At the second stage of synthesis, two related oleate complexes were decomposed using high-boiling solvents (1-octadecene) in the presence of oleic acid. The reaction time was one hour for the synthesis of compounds with different Mn content, the amount of OA was kept unchanged, and the reaction temperature was set to approximately 310°C. All compositions were synthesized under the same conditions and the same mixing rate. The resulting particles were separated from the solution using a permanent magnet and washed twice with ethanol and hexane, then dried in a drying cabinet at 55°C for 30 min and left to cool at room temperature. As a result, MNPs $Mn_xFe_{3-x}O_4$@OA were obtained (where $x = 0$, 0.25, 0.5, 0.75, 1.0).

2.2. Methods of studies of MNPs $Mn_xFe_{3-x}O_4$@OA ($x = 0, 0.25, 0.5, 0.75, 1.0$)

Structure and morphology of synthesized Mn particles$_xFe_{3-x}O_4$@OA were studied using X-ray diffraction and Mössbauer spectroscopy. Magnetic susceptibility was measured in an alternating magnetic field using a vibrating sample magnetometer (VSM). Determination of the atomic and crystal structure of synthesized MNPs $Mn_xFe_{3-x}O_4$@OA at room temperature was performed using an X-ray diffractometer (XRD) with scanning from 20 to 90 degrees (2θ) using radiation CuK_α ($\lambda = 0.154$ nm). Magnetic measurements in a constant magnetic field were carried out using a commercial superconducting quantum interference device (SQUID) Quantum Design.

Mössbauer spectroscopy was used to study the phase composition and magnetic state of synthesized MNPs. The Mössbauer spectra (MS) of samples of $Mn_xFe_{3-x}O_4$@OA were recorded using a spectrometer operating in constant acceleration mode with a triangular shape of the source velocity change relative to the absorber. The measurements were carried out in the geometry of transmission of gamma quanta through the studied sample from the source γ-radiation of Co-57 in the Rh matrix. The velocity scale was calibrated using a metal foil absorber α-Fe. Mathematical processing of experimental MS was carried out using a program using the least squares method and the Lorentz form of spectral lines, as well as the method of decoding the Mössbauer spectra by reconstructing the distributions of the parameters of the hyperfine interaction (HFI) [33]. Information on the phase composition and magnetic structure of the MNP was obtained from the analysis of the parameters of hyperfine interactions (HFI) and the probabilities of the distribution of effective magnetic fields calculated from experimental MS.

3. Results and discussion

3.1. X-ray diffraction analysis of MNP $Mn_xFe_{3-x}O_4$@OA

X-ray diffractograms (XRD) of synthesized samples of $Mn_xFe_{3-x}O_4$@OA are shown in Fig. 1, which indicates the characteristic peaks of 2θ for all synthesized samples at 30.0° (220), 35.65° (311), 43.24° (400), 53.64° (422), 62.59° (440) and 74.56° (533). The lines on the XRD are well aligned with the data for manganese ferrite indicated in the standard JCPDS card № 74−2399. The absence of additional lines on the XRD, which indicates a good crystallization of particles of a single-phase cubic spinel structure. The sizes of crystallites presented in Table 1 together with the parameters of the crystal lattice were calculated using the values of the maximum width of the diffraction line (311) according to the Scherer equation [13]. The large width of the diffraction peaks indicate the nanocrystalline nature of the synthesized particles. The peak (311) at $2\theta = 35°$ is characteristic of spinel ferrites.

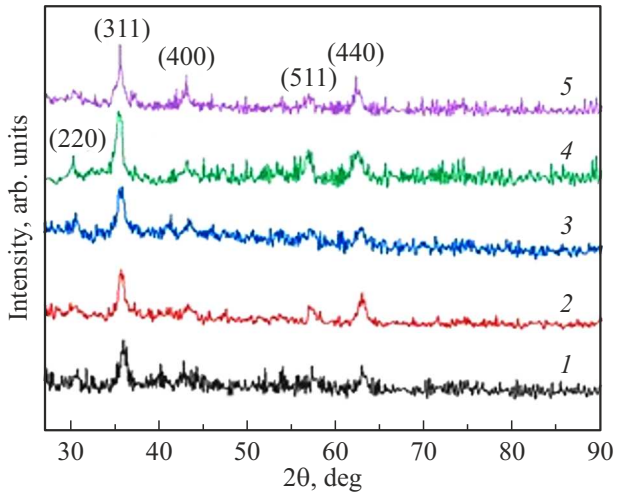

Figure 1. X-ray diffractograms (XRD) of MNPs $Mn_xFe_{3-x}O_4$@OA. Digit *1* denoted XRD at $x = 0$; *2* — at $x = 0.25$; *3* — at $x = 0.5$; *4* — at $x = 0.75$; and *5* — at $x = 1$.

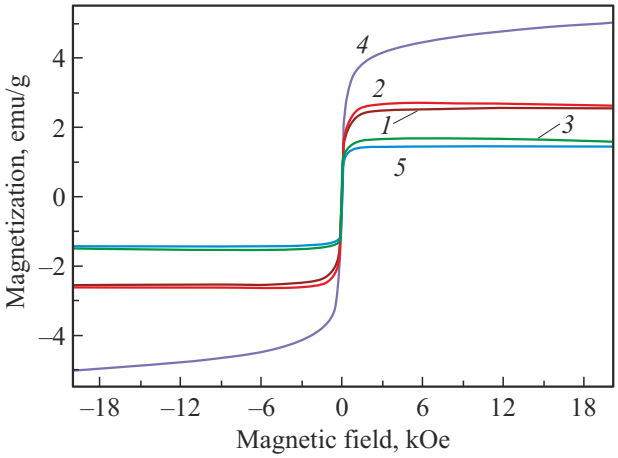

Figure 2. Saturation magnetization of MNP $Mn_xFe_{3-x}O_4$@OA depending on the amount of ion doping Mn^{2+}. Digit *1* denotes the curve *Ms* at $x = 0$; *2* — at $x = 0.25$; *3* — at $x = 0.5$; *4* — at $x = 0.75$ and *5* — at $x = 1$.

For MNPs of Fe_3O_4, the lattice cell parameter was 8.296 (2) Å. This is lower than that of bulk magnetite crystals (8.38−8.42 Å), but agrees close to the value of 8.35 Å for MNP Fe_3O_4 [34]. An expansion of the lattice cell to 8.391 Å is observed with an increase of the amount of Mn, and a possible explanation for this is that the radius of the introduced ions Mn^{2+} is 0.91 Å, which is greater than the radii of the substituted ions Fe^{2+} (0.80 Å) and/or Fe^{3+} (0.63 Å) [35].

3.2. Magnetic characteristics of Mn nanoparticles$_x$Fe$_{3-x}$O$_4$@OA

Studies of such important magnetic characteristics as saturation magnetization (Ms) and coercivity (Hc) depending on particle sizes, on the number of Mn ions in $Mn_xFe_{3-x}O_4$, a number of works are devoted to the thickness and hydrophobicity of the coating [17,22,29,30,32]. Thus, it was found that the value of Ms in the particles of $Mn_xFe_{3-x}O_4$ increases with an increase of the number of Mn ions [29], whereas a decrease was found Ms in [30]. With an increase in the number of Mn ions in the functionalized particles of $Mn_xFe_{3-x}O_4$@PEG, an increase in the number of Mn leads to a decrease in Ms to 31.33 emu/g [36], in $Mn_xFe_{3-x}O_4$@PVP, the value of Ms drops to 31.86 emu/g [32]. The increase of the coating thickness from 0 to 50% in Fe_3O_4@PEG lowers the value of Ms from 77.16 to 37.15 emu g^{-1} [37].

Table 1. Characteristics of MNP $Mn_xFe_{3-x}O_4$@OA at 300 K. The values D_{RD} and α_{RD} were obtained from X-ray diffractograms, the remaining parameters from magnetic measurements

Sample x	D_{RD} (nm)	α_{RD} (Å)	Dm (nm)	Ms (emu/g)	Mr (emu/g)	Hc (Oe)	α_m (Å)
0.0	11.11	8.296	13.18	2.56	0.38	16.21	0.829
0.25	11.50	8.351	11.19	2.67	0.44	19.6	0.839
0.5	9.10	8.340	13.11	1.58	0.23	11.69	0.838
0.75	17.39	8.39	11.19	5.09	0.43	10.9	0.839
1.0	10.08	8.41	13.03	1.42	0.32	4.9	0.838

Dependences of Ms on the concentration of Mn ions in synesized MNP $Mn_xFe_{3-x}O_4$@OA obtained using a physical property measurement system (PPMS) in magnetic fields up to 2 T, are shown in Fig. 2. Diameters (Dm) of magnetic nanoparticles $Mn_xFe_{3-x}O_4$@The OA calculated from the dependencies Ms (Fig. 2) are given in Table 1, which also shows the values of Ms depending on the number of ions Mn^{2+}. All magnetization curves (Fig. 2) have a *S*-shaped shape, and the samples exhibit typical superparamagnetic behavior. Level Ms of synthetized Mn nanoparticles$_x$Fe$_{3-x}$O$_4$@OA is sufficient for use in biomedicine.

4. Experimental Mössbauer spectra of MNP $Mn_xFe_{3-x}O_4$@OA and their analysis

Mössbauer spectroscopy (MSp) a unique method based on non-redundant resonant absorption of γ-radiation is a probe for both structure and magnetism at the local level [13,14,19,24,38]. The high selectivity of MSp to Fe^{2+} and Fe^{3+} ions, to the environment of Fe atoms, allows extracting information about the structure, valence state, stoichiometry, types of coordination and magnetic ordering, phase transitions and phase components both in qualitative and in quantitatively, even if the phases are present in small quantities. MSp uniquely identifies iron oxides (hematite,

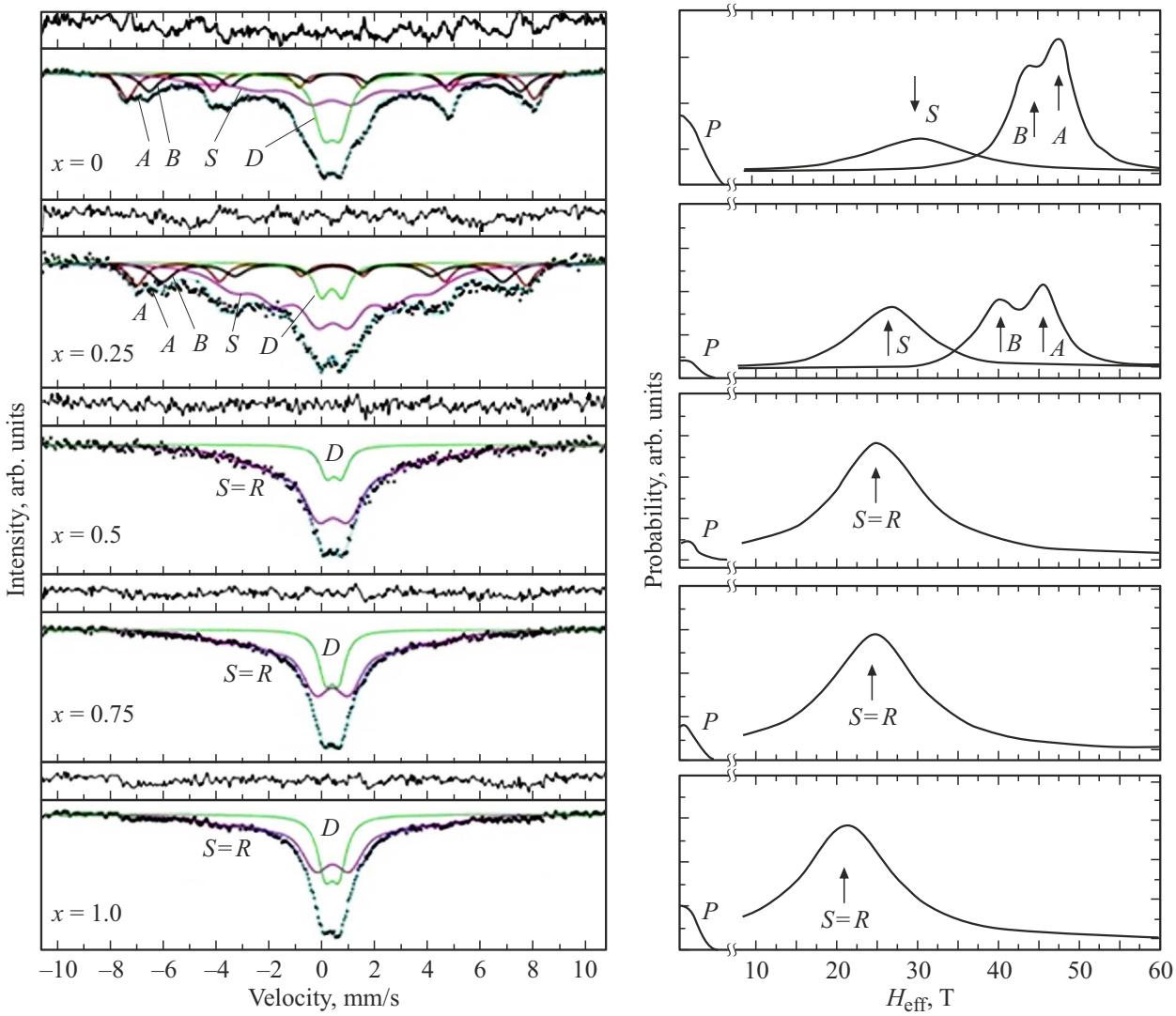

Figure 3. *a* — Mössbauer spectra of $Mn_xFe_{3-x}O_4$@OA obtained at room temperature and their model representations obtained using the program [33]. The difference between experimental and model values is shown above each spectrum. Sextiplets denoted as *A* are related to Fe ions in (*A*), *B* — to Fe ions [*B*] sublattices, *D* — ions of Fe particles in the paramagnetic phase. *S* — Zeeman sextiplets of Fe ions in the surface layer of particles. $S = R$ — absorption lines formed by the surface layer of the particle and relaxation effects, *b* — functions $P(H_{eff})$ reconstructed from experimental Mössbauer spectra of MNP $Mn_xFe_{3-x}O_4$@OA using the program [33].

magnetite, maghemite, etc.), which is not available to other known methods. The short measurement time (10^{-8} s) makes the MSp sensitive to the relaxation effects of [39,40].

The Mössbauer spectra (MS) MNP $Mn_xFe_{3-x}O_4$@OA ($0 \le x \le 1$) obtained at room temperature without an external magnetic field and in a magnetic field are shown in Fig. 3, *a* and 4, *a* respectively. As can be seen in Fig. 3, *a* and 4, *a*, MS of MNP $Mn_xFe_{3-x}O_4$@OA have wide lines of Zeeman sextiplets (ZS), which complicates the analysis of spectra. Therefore, a complex procedure was used to fit the probability functions of the distribution of parameters of HFI and recover them from MS to process experimental MNP MS of $Mn_xFe_{3-x}O_4$@OA, [33]. The process of such fitting included: (1) a set of sextiplets with relaxation times greater than the limit of the time window of the experiment (10^{-8} s), and, consequently, blocked particles are found, (2) quadrupolar doublets formed from superparamagnetic particles whose relaxation times are less than the value of the time window (10^{-8} s), and (3) ZS with wide lines whose relaxation times are intermediate. The analysis of the curves $P(H_{eff})$ allows finding the components of sextiplets (and doublets) and drawing conclusions about the relation of these components to the corresponding iron oxides and the positions of Fe ions in the crystal lattice [13,14,19,24,38]. Deviation value ($\chi 2$) used to describe experimental The MS of the model components determines the accuracy of the fit, which in our cases was in the range from 1.1 to 1.2, which indicates a good match of the models used with experimental data and, consequently, the reliability of such processing.

4.1. Mössbauer measurements at room temperature without external magnetic field

The Mössbauer spectra (MS) of MNPs $Mn_xFe_{3-x}O_4$@OA, $(0 \le x \le 1)$ obtained at room temperature without superposition of a magnetic field are shown in Fig. 3, *a*. It should be noted that the obtained MS (Fig. 3, *a*) are similar to the experimental MS presented in [19,21,24,30,41–52]. The experimental values are shown in Fig. 3, *a* by dots, and the model components obtained by mathematical processing of experimental spectra using the program [33] are shown by solid lines.

MS of MNP $Mn_xFe_{3-x}O_4$@OA (Fig. 3, *a*), at $x = 0$ is significantly wider than that of stoichiometric bulk crystals Fe_3O_4 at temperatures of 300 K [53,56] and change greatly with the increase of the number of Mn ions from 0 to 1.0. A doublet is observed against the background of wide lines of ZS on MS of particles of $Mn_xFe_{3-x}O_4$@OA at $x = 0$ and 0.25, the intensity of which increases with the increase of concentration of Mn ions, while the intensities and magnitudes of the effective fields of the sextiplets decrease.

Mathematical processing of experimental MS of $Mn_xFe_{3-x}O_4$@OA (at $x = 0$; 0.25) was carried out using the program [33] taking into account the following circumstances. In magnetite (Fe_3O_4), Fe^{2+} ions occupy two nonequivalent crystallographic positions: tetrahedral — (*A*) and octahedral — [*B*], wherein the ions Fe^{2+} occupy half of the [*B*] nodes, and the ions Fe^{3+} are evenly distributed over positions [*B*] and (*A*). Consequently, the MS of magnetite at room temperature should consist of three Zeeman sextiplets belonging to iron ions in (*A*) and [*B*] positions [38,54]. Iron ions Fe^{3+} and Fe^{2+} [B] positions at temperatures above the Verwey point [54] equal to 119 K are in a state of electronic exchange, and they can be referred to as cations $Fe^{2.5+}$, which corresponds to one partial CC, and the other sextiplet belongs to the ions Fe^{3+} in (*A*) positions [38.54]. The value of $T\upsilon$ decreases when doped with even a small amount of metal ions [56], which allows processing MS of MNP $Mn_xFe_{3-x}O_4$@OA (when $x = 0$; 0.25) using a model consisting of two ZS and a doublet. However, such a model did not agree with experimental MS and a third Zeeman sextiplet was included in the spectrum analysis. As a result, a good match with the experimental MS at $x = 0$ and 0.25 was obtained using the model of three Zeeman sextiplets and one doublet. This is confirmed by the minimum values of the difference between the model and experimental values indicated above each spectrum (see Fig. 4, *a*), as well as values $\chi 2$, ranging from 1.1 to 1.2. Spectra of MNP of $Mn_xFe_{3-x}O_4$@OA at $x = 0.5$; 0.75 and 1.0 were processed using a model consisting of one ZS and one doublet.

The HFI parameters were calculated using the positions of spectral lines in MS of MNP $Mn_xFe_{3-x}O_4$@OA: isomeric shifts (IS), quadrupole splits (QS), effective fields (H_{eff}), presented in Table 2. The relative amounts of iron ions in the sublattices in MNP of $Mn_xFe_{3-x}O_4$@OA were determined based on the relative intensities of the sextiplet and doublet lines in MNP MS and were listed in Table 2. The ions Fe^{3+} and Fe^{2+} are uniquely identified in MS by their chemical shifts amounting to $\sim 0.2 \div 0.5$ mm/s and $\sim 0.9 \div 1.1$ mm/s, respectively [13,14]. Table 2 shows that the values of IS are within the range of $0.2 \div 0.4$ mm/s, indicating the presence in the studied MNPs of $Mn_xFe_{3-x}O_4$@OA only high-spin ions Fe^{3+}.

The observed broadening of the ZS lines in MS of spinel ferrite macrocrystals was first explained by the random distribution of cations by (*A*) nodes [53], leading to the formation of several octahedral [*B*] positions differing in the occupation density. Values of the effective fields of Fe ions in (*A*) SF nodes having twelve nearest neighbors in [*B*] positions depend on the number of magnetic cations in the [*B*] sublattice and, therefore, are less dependent on the random distribution of cations in [*B*] positions. The nearest neighbors of Fe ions in [*B*] positions are only six cations in (*A*) nodes, so the random distribution of magnetic cations by (*A*) nodes significantly more affects the effective ion fields of Fe [*B*] sublattices [53]. Based on the above, the ZS in MNP of $Mn_xFe_{3-x}O_4$@OA (Fig. 3, *a*) with the largest effective field was attributed to iron ions occupying in the crystalline SF lattice (*A*) positions, and sextiplets with smaller magnitudes H_{eff} — to Fe ions in [*B*] positions.

There is a sextiplet *S* with a line width twice as large (Table 2) as the lines (*A*) and [*B*] positions, and with a significantly smaller value H_{eff} in addition to the sextiplets of Fe ions (*A*) and [*B*] ions on MS of $Mn_xFe_{3-x}O_4$@OA (Fig. 3, *a*). Similar MS were observed in [19,21,24,30,41,41–52], however, the origin of such a sextiplet was explained in different ways. The formation of such a ZS in [48] was attributed to small accumulations of Fe ions during grinding, but no signs of such an accumulation were observed on the XRD. The occurrence of a sextiplet of the type *S* is explained by the relaxation effects in [39,40,42,47,50] or by the distribution of Fe and Mn ions over the sublattices [30].

The amount and, consequently, the role of iron ions located in the surface layer significantly increases in nanoparticles. There are approximately 0.15%, 20% and 60% of the atoms of the composition, respectively, in particles with a diameter of 1 μm, 6 nm and 1.6 nm on the surface [57]. In the case of Mössbauer spectroscopy, the Fe ions of the surface layer significantly increase the non-sufficient absorption of gamma quanta, and, consequently, the intensity of Mössbauer lines, compared with those located in the particle volume. This is the reason for the observation of significant differences between the MS of large and small particles [19,21,49] and, as suggested in [49,52,58], it can form spin-glass or „magnetically dead“ phases.

For the first time, the existence of a canting structure of magnetic spins in nanoparticles was shown by the Mössbauer spectroscopy of MNPs in strong external magnetic fields [59], then the moments in the volume are arranged collinearly (a structure of the Neel type). The results

Table 2. HFI parameters for MNP $Mn_xFe_{3-x}O_4$@OA obtained from Mössbauer spectra taken in the absence of an external magnetic field: Zeeman sextiplets denoted as *A*, *B* and *S*, doublets — *D* and relaxation components — *R*. Widths of the first and sixth lines ($G1$) of the Zeeman splitting, isomeric shifts (IS), quadrupole splitting (QS), effective magnetic fields (H_{eff}) and subspectral areas (S_p) calculated from MS of MNP $Mn_xFe_{3-x}O_4$@OA

x	Component	$G1$(mm/s)	IS(mm/s)	QS(mm/s)	H_{eff}(T)	S_p(%)
0	*A*	0.711 + / − 0.004	0.384 + / − 0.015	0.007 + / − 0.022	47.67 + / − 0.11	19
	B	0.822 + / − 0.143	0.405 + / − 0.010	0.105 + / − 0.020	43.46 + / − 0.09	16
	S	2.364 + / − 0.427	0.327 + / − 0.033	0.066 + / − 0.056	30.53 + / − 0.60	42
	D	0.873 + / − 0.044	0.369 + / − 0.005	0.634 + / − 0.016	–	23
0.25	*A*	0.711 + / − 0.004	0.365 + / − 0.021	0.024 + / − 0.042	45.58 + / − 0.17	15
	B	0.983 + / − 0.000	0.399 + / − 0.000	0.031 + / − 0.000	39.87 + / − 0.00	16
	S	1.877 + / − 0.000	0.384 + / − 0.000	0.042 + / − 0.000	25.16 + / − 0.00	60
	D	0.659 + / − 0.000	0.365 + / − 0.000	0.780 + / − 0.000	–	9
0.5	$S = R$	2.091 + / − 0.004	0.443 + / − 0.055	−0.213 + / − 0.100	24.37 + / − 0.84	87
	D	0.590 + / − 0.120	0.365 + / − 0.020	0.520 + / − 0.043	–	13
0.75	$S = R$	2.091 + / − 0.004	0.361 + / − 0.024	0.039 + / − 0.045	23.59 + / − 0.35	79
	D	0.605 + / − 0.031	0.372 + / − 0.005	0.493 + / − 0.011	–	21
1.0	$S = R$	2.091 + / − 0.004	0.389 + / − 0.020	−0.002 + / − 0.038	21.25 + / − 0.31	71
	D	0.671 + / − 0.024	0.369 + / − 0.003	0.517 + / − 0.008	–	29

obtained in [59] have been confirmed (see [38,60] and links there).

It should be noted that studies of the structure and properties of the surface layer of macrocrystals and nanoparticles attracted attention in the 1970s (see [61] and references there). To study the properties of a thin surface layer and the volume of macroscopic crystals, the method of simultaneous gamma-ray, X-ray and electron Mössbauer spectroscopy (SGXEMS) [62,63] was developed simultaneously. Later, the SGXEMS method was named in foreign literature as „Simultaneous Triple Radiation Mössbauer Spectroscopy" (STRMS) [64]). The direct experimental data with the use of SGXEMS for the first time proved the existence on the surface of ferromagnetic crystals Fe_3BO_6 of a thin transition layer in which magnetic moments smoothly change orientation from the direction in the volume to the direction on the surface [61]. Studies of ferrimagnetic highly anisotropic hexaferrite crystals ($BaFe_{12}O_{19}$) using the SGXEMS method have shown that such a transition layer can exist in a surface layer with a thickness of no more than 10 nm [65]. This is significantly less than the experimental accuracy of ~ 10 nm, but coincides with the value obtained from theoretical calculations by Neel [66]. The introduction of diamagnetic Sc and Al ions into the structure of the hexaferrites BaM and SgM, respectively, leads to an additional decrease in super-exchange interactions on the surface, as a result of which a surface layer is observed in the macrocrystals of BaScM and SrAlM, in which the orientation of the moments differs from the orientation in the volume [67–71]. It can be assumed that a similar pattern of changes in the orientation of moments also occurs on the surface of nanoparticles of $Mn_xFe_{3-x}O_4$@OA, called a canting structure and observed when strong magnetic fields are applied [59,60].

Thus, the deviation of the orientation of the moments observed in the surface layer of macrocrystals [61,67–71] should be preserved when the crystal sizes decrease to nanoparticles, From Table 2 it can be seen that at $x = 0$ and 0.25 the difference in values H_{eff} [*B*] sublattices and sextiplets *S* are significantly larger than when replacing in the immediate environment [*B*] ions of one Fe ion with a diamagnetic [53]. The large line widths of the sextiplet *S* and the large difference in the effective fields of *S* and [*B*] sextiplets allow us to assert that the sextiplet *S* belongs to Fe ions in the surface layer whose magnetic moments are found in a canting state.

An additional contribution to the sextiplet *S* can be made by Fe ions of the superparamagnetic state (SP) arising from collective magnetization fluctuations [39,40]. The measurement time (τ) in the Mössbauer method is $\sim 10^{-7}$ s, which makes it possible to record relaxation phenomena of smaller particles with shorter relaxation times. MS of SF particles with relaxation times $\tau > \tau_L$ (here τ_L — time of Larmor precession of the nucleus) consists of sextiplets with wide lines, and at $\tau < \tau_L$, the collapse of sextiplets into a superparamagnetic doublet is observed. The absence of a

part of super-exchange interactions in the surface layer leads to the fact that relaxation phenomena in the MNP should primarily occur in the surface layer.

The evolution of MS of MNP $Mn_xFe_{3-x}O_4$@OA when the number of ions changes Mn from 0 to 1 can be explained as follows. The iron ions located on the surface of the particles lack some of their magnetic neighbors, which leads to a decrease in the super-exchange interactions of surface ions and the formation of a ZS, designated as S, belonging to the Fe ions of the surface layer and indicating the existence of a canting spin structure on the surface of the MNP. The observed doublets on MS (Fig. 3, a) at $x = 0$ and 0.25 result from the relaxation effects. The intensity of the doublet decreases at $x = 0.25$ due to the intensification of relaxation processes and the formation of the relaxation „stiplet", possibly contributing to the lines S. A further increase of the concentration of Mn ions ($x > 0.5$) additionally destroys super-exchange bonds and enhances relaxation effects in the surface layer of MNPs. At the same time, sextiplet lines S are observed on the MS of particles of $Mn_xFe_{3-x}O_4$@OA (Fig. 3, a) together with a paramagnetic doublet, probably with a contribution from relaxation phenomena, indicated in Fig. 3, a as $S + R$. This means that together with the canting structure of magnetic moments, a superparamagnetic state is formed in the surface layer of particles. The thickness of such a surface layer increases with an increase in the number of Mn ions, as indicated by an increase in the intensity of the line $R + S$ in Fig. 3, b. Consequently, MNP $Mn_xFe_{3-x}O_4$@OA are core/shell type particles in which the surface layer (shell) has a canting magnetic structure, relative to the ferrimagnetic (non-Aelian) ordering of the volume (core) of crystallites.

It should be noted that the state with different magnetic structures of the volume and surface layer of single-phase MNP ferrites-spinels cannot be detected by other known methods, for example, electron microscopy or other methods, except by the method of Mössbauer spectroscopy. It is explained by the fact that MNPs of ferrite-spinels are single-phase, well crystallized in the form of particles from a single material. The latter distinguishes SF particles from MNPs of the core/shell type, in which the core and shell consist of different magnets, for example, magnetite and maghemite [72].

4.2. Analysis of distribution functions H_{eff} MNP $Mn_xFe_{3-x}O_4$@OA

It should be noted that the local heterogeneity of the distribution of cations in the MNP of substituted SF significantly complicates the interpretation of MS. Therefore, due to the lack of resolution of sextiplets, MS processing by Lorentz lines to obtain the distribution functions of the effective magnetic field $P(H_{\text{eff}})$ is not effective. In such cases, the most reliable method is the MS analysis using the Voigt function as a spectral line [73,74], therefore, functions $P(H_{\text{eff}})$ were recovered from experimental MS of MNP $Mn_xFe_{3-x}O_4$ using the Voigt function as the functions of the spectral line [33] (Fig. 3, b). The obtained functions $P(H_{\text{eff}})$ differ from the curve $P(H_{\text{eff}})$ of magnetite macrocrystals, on which two maxima belonging to iron ions in two nonequivalent sublattices are observed.

Analysis of functions $P(H_{\text{eff}})$ obtained from MS of MNP $Mn_xFe_{3-x}O_4$@OA (Fig. 3, a) showed that at $x \leq 0.25$ three peaks can be distinguished in the area of fields from 20 to 55 T, designated as A, B and S. The range from 0 to 5 T corresponds on MS to doublet lines related to the fraction of particles in the paramagnetic state and the probability of their presence, as can be seen in Fig. 3, b, decreases at $x = 0.25$ (associated, apparently, with the intensification of relaxation processes), and then increases as the number of Mn ions increases. The peaks indicated on $P(H_{\text{eff}})$ as A and B (Fig. 4, b) belong to the lines ZS belonging to the ions Fe in (A) and $[B]$ positions, respectively. The nature of the line S and $S + R$ was discussed above. The increase of the number of Mn ions leads to a shift of the positions of the peaks A and B towards the smaller H_{eff} and a decrease in the probability of the presence of these lines (Fig. 3, b), indicating that the proportion of the magnetically ordered state of particles decreases. At the same time, the probability of the line $S + R$ increases, which means an increase in the proportion of the surface with a canting magnetic structure and relaxation effects. An increase of the probability of the line P indicates an increase of the number of particles in the paramagnetic state.

Features of the functions $P(H_{\text{eff}})$ reflect the complex magnetic structure of the MNP $Mn_xFe_{3-x}O_4$@OA, which cannot be explained only by a change in the distribution of ions over nonequivalent positions when introducing Mn ions, but it is necessary to take into account the significant impact of surfaces.

4.3. Mössbauer studies of MNP $Mn_xFe_{3-x}O_4$@OA in an external magnetic field with a strength of 1.7 kOe

Using strong (tens of kOe) external magnetic fields in the Mössbauer studies allowed obtaining direct evidence of the existence of a canting structure of magnetic moments of Fe [59] ions in the surface layer of the MNP. Strong external magnetic fields are also used in Mössbauer spectroscopy to obtain information about the distribution of ions across the sublattices of SF [38,60].

Currently, the Mössbauer studies of the impact of weak magnetic fields (in the order of units 1 kOe or less) on the properties of MNPs [76], begun in the late 60 s [75], are relevant. This is caused by the requirement to understand the influence of weak magnetic fields on the properties of MNPs associated with their use for hyperthermic therapy of malignant tumors [18,57]. From the MS obtained by applying weak magnetic fields (with a strength of hundreds of Oe), it is possible to extract information about the dynamic effects associated with the processes of

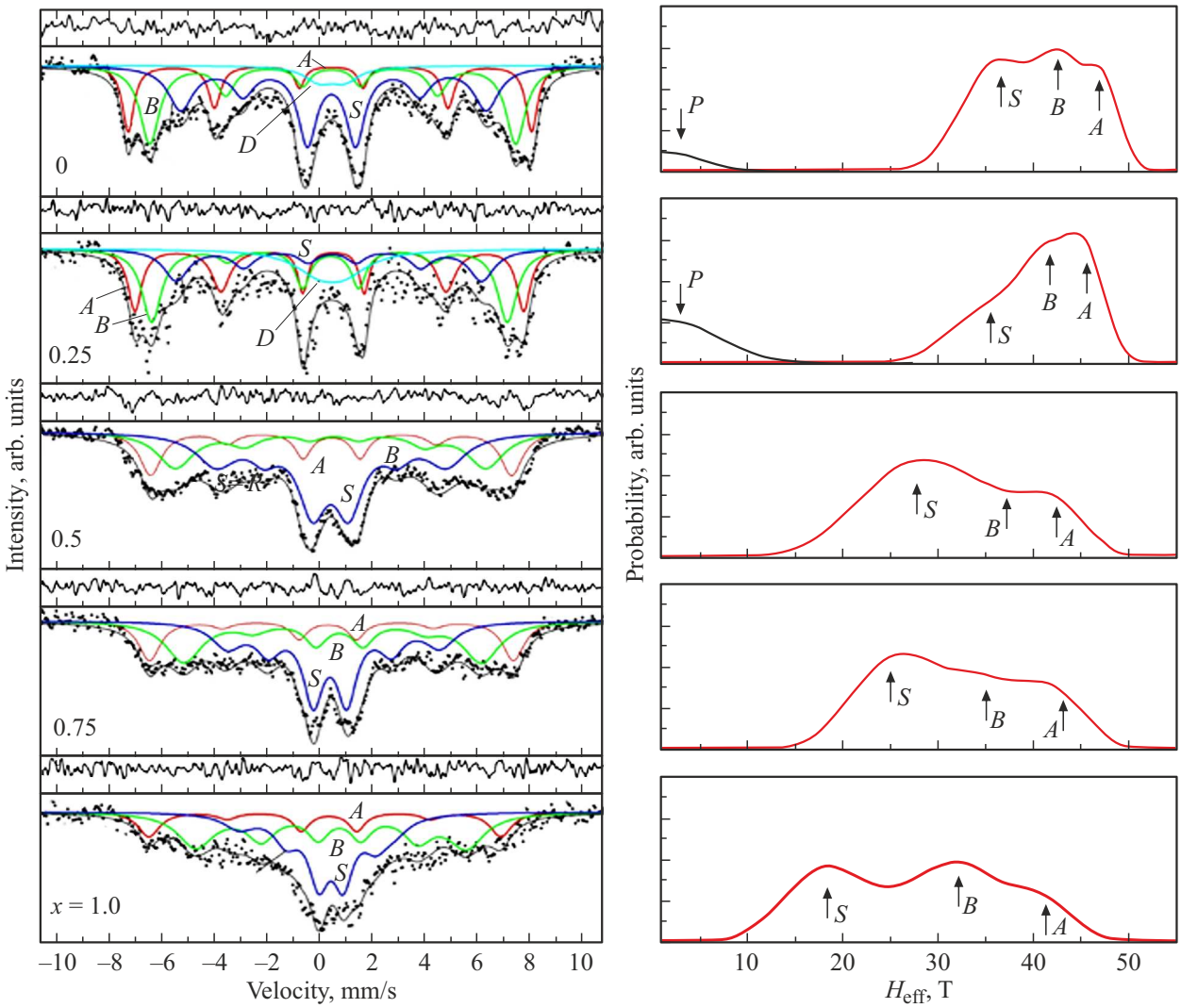

Figure 4. *a* — experimental Mössbauer spectra of MNP $Mn_xFe_{3-x}O_4$@OA (at $x = 0$; 0.25; 0.5; 0.75 and 1.0) obtained at room temperature in an external magnetic field with a strength of 1.7 kOe. The difference between experimental and model values is shown above each spectrum. The model Zeeman sextiplets obtained using the program [33] are designated *A*, *B*, *S*. *b* — distribution functions of effective magnetic fields $P(H_{eff})$ obtained from experimental spectra of $Mn_xFe_{3-x}O_4$@OA using the program [33].

magnetic moment fluctuation and transition to paramagnetic state [76]. Therefore, Mössbauer measurements of MNP $Mn_xFe_{3-x}O_4$@OA of room temperature were carried out with a magnetic field with a strength of 1.7 kOe applied parallel to the gamma radiation beam. The obtained experimental MS are shown in Fig. 4, *a*. Using the procedure [33] MS were decomposed into partial sextiplets and doublets shown by solid lines in Fig. 4, *a*. Recovered from MS (Fig. 4, *a*) functions $P(H_{eff})$ and calculated parameters of HFI are presented in Fig. 4, *b* and in the Table 3 respectively.

The resolution of spectral lines of MS of MNP $Mn_xFe_{3-x}O_4$@OA (Fig. 4, *a*) is better than lines of MS without an external field (Fig. 3, *a*), because the intensities of the second and fifth lines of ZS (Fig. 4, *a*) have significantly decreased due to the parallelism of the magnetic field to the gamma radiation beam. The intensity of the ZS lines decreases with an increase of the quantity of Mn, the values of the splitting of the ZS decrease and the sextiplets gradually „close“, but do not disappear completely. At the same time, the line intensities in the zero velocity region increase. All this means that in the studied particles, the superimposition of a magnetic field with a strength of 1.7 kOe leads to stabilization, but not to complete suppression of superparamagnetic behavior in the studied samples.

The MS analysis (Fig. 4, *a*) using the program [33] showed that the obtained spectra can be modeled using three Zeeman sextiplets. Sextiplets *A* and *B* are related to iron ions of (*A*) and [*B*] positions. The widths of lines *S* and $S + R$ are large enough to be explained by the contribution of [*B*] iron ions, which lack one exchange bond. The difference in the values of the effective fields of *B* and *S* sextiplets is greater than the differences in H_{eff} arising

Table 3. HFI parameters for MNP $Mn_xFe_{3-x}O_4$@OA, taken in an external magnetic field with a strength of 1.7 kOe, calculated from Zeeman splits, denoted as A, B, S and $S = R$, as well as doublets — D. Widths of the first and sixth lines $(G1)$ of the Zeeman splitting, isomeric shifts (IS), quadrupole splitting (QS), effective magnetic fields (H_{eff}) and subspectral areas (S_p)

x	Component	$G1$ (mm/s)	IS (mm/s)	QS (mm/s)	$H_{\text{eff}}(T)$	S_p (%)
0	A	0.526 + / − 0.036	0.338 + / − 0.008	0.051 + / − 0.016	47.50 + / − 0.06	21
	B	0.882 + / − 0.084	0.399 + / − 0.013	0.040 + / − 0.025	43.09 + / − 0.09	31
	S	1.144 + / − 0.187	0.409 + / − 0.012	0.076 + / − 0.024	33.97 + / − 0.04	42
	D	1.354 + / − 0.299	0.383 + / − 2.974	0.983 + / − 0.263	–	6
0.25	A	0.621 + / − 0.084	0.369 + / − 0.015	0.162 + / − 0.029	45.78 + / − 0.15	31
	B	0.882 + / − 0.084	0.319 + / − 0.023	0.043 + / − 0.046	41.87 + / − 0.19	33
	S	1.144 + / − 0.187	0.335 + / − 0.047	0.122 + / − 0.087	31.97 + / − 0.04	21
	D	2.252 + / − 0.384	0.383 + / − 2.974	0.983 + / − 0.263	–	15
0.5	A	0.987 + / − 0.099	0.367 + / − 0.015	0.016 + / − 0.031	42.50 + / − 0.10	22
	B	1.666 + / − 0.375	0.409 + / − 0.034	0.144 + / − 0.060	36.56 + / − 0.30	25
	S	1.814 + / − 0.276	0.352 + / − 0.016	0.024 + / − 0.031	27.08 + / − 0.47	53
0.75	A	0.987 + / − 0.099	0.303 + / − 0.019	0.138 + / − 0.037	42.85 + / − 0.12	20
	B	1.666 + / − 0.375	0.545 + / − 0.021	0.259 + / − 0.038	35.05 + / − 0.19	35
	S	1.399 + / − 0.758	0.384 + / − 0.019	0.138 + / − 0.035	25.05 + / − 0.22	46
1.0	A	0.987 + / − 0.099	0.201 + / − 0.041	0.154 + / − 0.076	41.44 + / − 0.30	17
	B	1.666 + / − 0.375	0.514 + / − 0.035	0.323 + / − 0.065	31.85 + / − 0.33	43
	S	1.399 + / − 0.758	0.075 + / − 0.079	0.555 + / − 0.156	18.25 + / − 0.55	40

from the loss of $[B]$ ion of one exchange interaction. It can be argued that the ZS belongs to Fe ions occupying positions in the surface layer, as described above. However, the contribution of relaxation effects to this sextiplet cannot be excluded.

Functions $P(H_{\text{eff}})$ obtained from MS of MNP $Mn_xFe_{3-x}O_4$ in a magnetic field can be described by three peaks indicated in Fig. 4, *a* arrows A, B and S and $S + R$. A line (P) belonging to the paramagnetic phase is observed at $x = 0$ and 0.25 in the range from 0 to 10 T. An increase in the concentration of Mn ions $(x > 0.25)$ leads to the disappearance of the paramagnetic peak. This can be explained by the fact that smaller particles in the paramagnetic state are present in the samples at substitution values $x < 0.25$. The magnitude of the external magnetic field at $x > 0.25$ is sufficient to stabilize the magnetic state of smaller particles and the contribution to MS from such particles coincides with the relaxation in the ZS, denoted as $S + R$.

Thus, the Mössbauer studies in magnetic fields also indicate that MNP $Mn_xFe_{3-x}O_4$@OA have a core/shell type structure described above. The Mössbauer data of the studied MNP $Mn_xFe_{3-x}O_4$@OA showed that they are in a superparamagnetic state, which is required for hyperthermic treatment of malignant tumors

5. Estimation of the size of MNP $Mn_xFe_{3-x}O_4$@OA

The sensitivity of the Mössbauer spectroscopy makes it possible to determine the size of magnetic nanoparticles. Thus, well-resolved lines of nonequivalent sublattices are observed on the MS of Fe_3O_4 nanoparticles with dimensions

36 nm [77], with dimensions 25 nm [78], whereas sextiplets of unequal positions of Fe ions are not allowed in the obtained MS of MNP Fe_3O_4 with sizes 9 nm [77] and 12 nm [45]. MS of Fe_3O_4 with dimensions of 7 nm consists of ZS with wide unresolved lines (A) and [B] ion positions Fe [78]. Doublets are observed on MS of MNP Fe_3O_4 with sizes 3 nm [79], sizes from 5.3 to 10.6 nm [80], as well as sizes 5.0 nm, [81], indicating the paramagnetic state of the particles. The MS obtained with the particle size Fe_3O_4@OA 11 nm with oleanite coating (4 mmol) [24] is similar to that shown in Fig. 3, *a* for $x = 0$. An increase in oleanite to 16 mmol leads to the formation of MS macroscopic magnetite [24].

Doublets or paramagnetic state is also observed in $MnFe_2O_4$ particles with sizes 4.7 nm [82] and 7.8 nm [50]. If the MS of particles $Mn_{0.5}Fe_{2.5}O_4$ with a size of 9.3 nm consists of a doublet and a low-intensity sextiplet of lines, then the intensity of the lines of the sextiplet increased on MS of MNP $Mn_{0.25}Fe_{2.75}O_4$ with size 9.5 nm [83]. MS with weak resolution of the lines of nonequivalent positions of Fe ions were obtained for particles of $Mn_xFe_{3-x}O_4$@OA with dimensions of 6.8 nm [84]. For $MnFe_2O_4$ particles with sizes from 20 to 68 nm and sizes 42 nm in [84,85], respectively, MS with narrow well-resolved sextiplets of nonequivalent positions of Fe ions were obtained. MS of MNP $MnFe_2O_4$ with dimensions of 10 nm consist of sextiplets with wide intense lines against which a doublet [86] is observed. MS with resolved interstiplets of nonequivalent positions of Fe ions were obtained for MNP $Mn_xFe_{3-x}O_4$ with a size from 30 to 40 nm [87]. MS of particles $Mn_{0.5}Fe_{2.5}O_4$ with dimensions of 10 nm are sextiplets with very wide lines[45].

Comparison of the obtained MS with the published ones and their analysis suggests that the average sizes of crystallites of $Mn_xFe_{3-x}O_4$@OA vary from 8 nm for Fe_3O_4@OA ($x = 0$) to 12 nm for $MnFe_2O_4$ ($x = 1.0$).

6. Conclusion

Systematic studies of the properties, phase composition and magnetic structure and magnetic of nanoparticles of $Mn_xFe_{3-x}O_4$@OA synthesized by thermal decomposition and functionalized with oleic acid were conducted. Experimental X-ray and Mössbauer data indicate that there are no impurity phases and MNP $Mn_xFe_{3-x}O_4$@OA are single-phase. It was found using XRD measurements that the average sizes of the crystallites of $Mn_xFe_{3-x}O_4$@OA vary from 11 to 18 nm with the increase of Mn concentration. Analysis of the Mössbauer spectra and comparison with published data showed that as the concentration of ions increases Mn average diameter of nanoparticles $Mn_xFe_{3-x}O_4$@OA varies from 8 to 12 nm. A paramagnetic doublet is observed on the Mössbauer spectra of particles at $x = 1.0$ against the background of a low-intensity sextiplet. The doublet refers to Fe ions located in smaller particles whose blocking temperature is below room temperature. The doping of magnetite with Mn ions leads to a decrease in the effective magnetic fields and magnetization of the samples.

The analysis of the Mössbauer spectra of MNP $Mn_xFe_{3-x}O_4$@OA and the distribution functions of effective magnetic fields on iron nuclei $P(H_{\text{eff}})$ showed that the studied nanoparticles they have a surface layer, the magnetic structure of which differs from the structure of the bulk part of the particle, i.e. on the surface of the MNP there is a so-called canting structure of the surface layer [59]. The reason for the formation of such a layer is the absence of a part of super-exchange bonds on the surface of nanoparticles. Thus, this paper showed for the first time (without the use of external magnetic fields) that the magnetic structure of the surface MNP is canting relative to the volume of particles while earlier the existence of a canting magnetic structure on the surface of the MNP was found by the Mössbauer spectroscopy of the MNP in strong magnetic fields (using expensive equipment). Thus it can be argued that MNP $Mn_xFe_{3-x}O_4$@OA are core/shell type particles. The data obtained show the complexity of the structure of nanoparticles $Mn_xFe_{3-x}O_4$@OA and allow us to explain the magnetic properties of such nanoparticles, which is important in the development and creation of MNPs for various applications, including for biomedicine.

Acknowledgments

N. Dogan and O.M. Dogan would like to thank the Scientific and Technological Research Council of Turkey (TUBITAK Grant No: 115E776) for supporting these research.

Conflict of interest

The authors declare that they have no conflict of interest.

References

[1] O. Kalogirou. Modern Ferrites: Emerging. Technologies and Applications. Biomedical Applications of Nanoparticle Ferrites / Ed. V.G. Harris. John Wiley & Sons Ltd. (2023). V. 2. Ch. 10. P. 347.
[2] L.S. Arias, J.P. Pessan, A.P.M. Vieira, T.M.T. de Lima, A.C.B. Delbem, D.R. Monteiro. Antibiotics **7**, 46 (2018). DOI: 10.3390/antibiotics7020046.
[3] V. Socoliuc, D. Peddis, V.I. Petrenko, M.V. Avdeev, D. Susan-Resiga, T. Szabó, R. Turcu, E. Tombácz, L. Vékás. Magnetochem. **6**, 2 (2020).
[4] N.V. Tkachenko, L.P. Olkhovik, A.S. Kamzin. FTT **53**, 1512 (2011). (in Russian).
[5] A.M. Granov, S.F. Vershinina, R.B. Samsonov, A.B. Markochev, V.I. Yevtushenko. Med. akad. zhurn., **17** (1), 82 (2017). (in Russian).
[6] L. Vékás. Adv. Sci. Technology **54**, 127 (2008). DOI: 10.4028/www.scientific.net/AST.54.127
[7] S.A. Novopashin, M.A. Serebryakova, S.Ya. Khmel. Teplofizika i aeromekhanika **22**, *4*, 411, (2015). (in Russian).

[8] O. Oehlsen, S.I. Cervantes-Ramírez, P. Cervantes-Avilés, I.A. Medina-Velo. ACS Omega **7**, 3134 (2022).
[9] S. Vinod, J. Philip. Adv. Colloid Interface Sci. **307**, 102729 (2022). https://doi.org/10.1016/j.cis.2022.102729.
[10] XVIII Mezhdunar. Plesskaya nauch. konf. po nanodispersnym magnitnym zhidkostyam. Tr. / Edited by Yu.B. Kazakov. Izdvo Ivanovskogo gos. energeticheskogo un-ta im. V.I. Lenina. ISBN 978-5-00062-343-5. 2018. 260 p. (in Russian).
[11] V.R. Khabibullin, G.V. Stepanov. Zhurn. fiz. khimii **93**, *7*, 1048 (2019). (in Russian).
[12] N. Dogan, O.M. Dogan, M. Irfan, F. Ozel, A.S. Kamzin, V.G. Semenov, I.V. Buryanenko. J. Magn. Magn. Mater. **561**, 169654 (2022). https://doi.org/10.1016/j.jmmm.2022.169654.
[13] A.S. Kamzin, G. Caliskan, N. Dogan, A. Bingolbali, V.G. Semenov, I.V. Buryanenko. FTT, **64**, 1570 (2022). (in Russian). DOI: 10.21883/FTT.2022.10.53107.391.
[14] A.S. Kamzin, G. Caliskan, N. Dogan, A. Bingolbali, V.G. Semenov, I.V. Buryanenko. ZhTF **92**, 1884 (2022). (in Russian).
[15] L.S. Ganapathe, M.A. Mohamed, R.M. Yunus, D.D. Berhanuddin. Magnetochem. **6**, 68 (2020). DOI: 10.3390/magnetochemistry6040068.
[16] S. Gul, S.B. Khan, I.U. Rehman, M.A. Khan, M.I. Khan. Front. Mater. **6**, 179 (2019).
[17] K.K. Kefeni, T.A.M. Msagati, T.T.I. Nkambule, B.B. Mamba. Mater. Sci. Eng. C **107**, 110314 (2020). https://doi.org/10.1016/j.msec.2019.110314.
[18] V. Narayanaswamy, S. Sambasivam, A. Saj, S. Alaabed, B. Issa, I.A. Al-Omari, M. Obaidat. Molecules **26**, 796 (2021). https://doi.org/10.3390/molecules26040796.
[19] T. Muthukumaran, S.S. Pati, L.H. Singh, A.C. de Oliveira, V.K. Garg, J. Philip. App. Nanosci. **8**, 593 (2018). https://doi.org/10.1007/s13204-018-0715-y.
[20] M. Abdolrahimi, M. Vasilakaki, S. Slimani, N. Ntallis, G. Varvaro, S. Laureti, C. Meneghini, K.N. Trohidou, D. Fiorani, D. Peddis. Nanomaterials **11**, 1787 (2021). https://doi.org/10.3390/nano11071787.
[21] R. Ghosh, L. Pradhan, Y.P. Devi, S.S. Meena, R. Tewari, A. Kumar, S. Sharma, N.S. Gajbhiye, R. K. Vatsa, B.N. Pandey, R.S. Ningthoujam. J. Mater. Chem., **21**, 13388 (2011).
[22] Z. Karimi, S. Abbasi, H. Shokrollahi, Gh. Yousefi, M. Fahham, L. Karimi, O. Firuzi. Mater. Sci. Eng. C**71** (2017) 504 p. http://dx.doi.org/10.1016/j.msec.2016.10.008.
[23] S.R. Mokhosi, W. Mdlalose, A. Nhlapo, M.I. Singh. Pharmaceutics **14**, 937 (2022). https://doi.org/10.3390/pharmaceutics14050937.
[24] U. Klekotka, D. Satuła, Simo Spassov, Beata Kalska-Szostko. Mater. **14**, 100 (2021). https://doi.org/10.3390/ma14010100.
[25] R.G.D. Andrade, S.R.S. Veloso, E.M.S. Castanheira. Int. J. Mol. Sci. **21**, 2455 (2020). DOI: 10.3390/ijms21072455.
[26] X. Liang, Y. Zhong, S. Zhu, H. He, P. Yuan, J. Zhu, Z. Jiang. Solid State Sci. **15**, 115 (2013). http://dx.doi.org/10.1016/j.solidstatesciences.2012.10.005. 1
[27] P. Saha, R. Rakshit, K. Mandal. J. Magn. Magn. Mater. **475**, 130 (2019). https://doi.org/10.1016/j.jmmm.2018.11.061.
[28] A.S. Korsakova, D.A. Kotsikau, Yu.S. Haiduk, V.V. Pankov. Condens. Matter Interphas. **22**, 466 (2020). DOI: https://doi.org/10.17308/kcmf.2020.22/3076.
[29] K. Rotjanasuworapong, W. Lerdwijitjarud, A. Sirivat. Nanomaterials **11**, 876 (2021). https://doi.org/10.3390/nano11040876
[30] Y.H. Li, T. Kouh, In-Bo Shim, Ch.S. Kim. J. App. Phys. **111**, 07B544 (2012). DOI: 10.1063/1.3687007.
[31] J. Lee, S. Zhang, S.H. Sun. Chem. Mater. **25**, 1293 (2013).
[32] M. Aghazadeh, I. Karimzadeh, M.R. Ganjali. Mater. Lett. **228**, 137 (2018). https://doi.org/10.1016/j.matlet.2018.05.087
[33] V.G. Semenov, V.V. Panchuk. Mössbauer Spectra Processing Software MOSWIN. Chast. soobschenie.
[34] N.C.C. Lobato, M.B. Mansur, A. de M. Ferreira. Mater. Res. **20**, 736 (2017). https://doi.org/10.1590/1980-5373-mr-2016-0707
[35] J. Dhumal, S.S. Bandgar, M. Phadatare, G.S. Shahane. Internat. J. Res. Anal. Rev. **6**, 1058 (2019).
[36] S. Sunaryono, M.F. Hidaya, N. Mufti, S. Soontaranon, A. Taufiq. J. Polymer Res. **27**, 284 (2020). https://doi.org/10.1007/s10965-020-02065-w.
[37] G. Antarnusa. Mater. Res. Express **7**, 056103 (2020). https://doi.org/10.1088/2053-1591/ab8bef
[38] Mössbauer Spectroscopy Applied to Magnetism and Material Science / Eds G.J. Long, F. Grandjean. Plenum Press, N.Y. (1993). 479 p.
[39] S. Morup, H. Topsoe. App. Phys. **11**, 63 (1976).
[40] M.A. Chuev. ZhETF **141**, 698 (2012). (in Russian).
[41] K.S. Al-Rashdi, H.M. Widatallah, F. Al Ma'Mari, O. Cespedes, M. Elzain, A. Al-Rawas, A. Gismelseed, A. Yousif. Hyperfine Interact. **239**, 3 (2018). https://doi.org/10.1007/s10751-017-1476-9.
[42] A. Alomari, H.M. El Ghanem, A.-F. Lehlooh, I.M. Arafa, I. Bsoul, Sensors Transducers **192**, 53 (2015).
[43] G.F. Goya, T.S. Berquo, F.C. Fonseca, M.P. Morales. J. Appl. Phys., **94**, 3520 (2003).
[44] V. Sepelak, A. Feldhoff, P. Heitjans, F. Krumeich, D. Menzel, F.J. Litterst, I. Bergmann, K.D. Becker, Chem. Mater. **18**, 3057 (2006).
[45] B. Kalska, J.J. Paggel, P. Fumagalli, J. Rybczynski, D. Satula, M. Hilgendorff, M. Giersig. J. App. Phys. **95**, 1343 (2004). DOI: 10.1063/1.1637134.
[46] S.H. Gee, Y.K. Hong, D.W. Erickson, M.H. Park. J. Appl. Phys. **93**, 7560 (2003).
[47] S.B. Singh, Ch. Srinivas, B.V. Tirupanyam, C.L. Prajapat, M.R. Singh, S.S. Meena, Pramod Bhatte, S.M. Yusuf, D.L. Sastry. Ceram. Int. **42**, 19188 (2016). http://dx.doi.org/10.1016/j.ceramint.2016.09.
[48] W.B. Dlamini, J.Z. Msomi, T. Moyo. J. Magn. Magn. Mater. **373**, 78 (2015). http://dx.doi.org/10.1016/j.jmmm.2014.01.066.
[49] M.I.A.A. Maksoud, A. El-Ghandour, G.S. El-Sayyad, R.A. Fahim, A.H. El-Hanbal, M. Bekhit, E.K. Abdel-Khale, H.H. El-Bahnasawy, M.A. El-Kodous, H. Ashour, A.S. Awed. J. Inorg. Organomet. Polym. Mater. **30**, 3709 (2020). doi.org/10.1007/s1090 4-020-01523-8.
[50] K.L. Zaharieva, Z.P. Cherkezova-Zheleva, B.N. Kunev, I.G. Mitov, S.S. Dimova. Bulgar. Chem. Commun. **47**, 261 (2015).
[51] E. Umut, M. Coşkun, H. Güngüneş, V. Dupuis, A.S. Kamzin. J Supercond. Nov. Magn. **34**, 913 (2021).
[52] S. Mørup, F. Bødker, P.V. Hendriksen, S. Linderoth. Phys. Rev. B **52**, 287 (1995).
[53] G.A. Sawatzky, F. Van Der Woude, A.H. Morrish. Phys. Rev. **187**, 747 (1969).
[54] L. Häggström, H. Annersten, T. Ericsson, R. Wäppling, W. Karner, S. Bjarman, Hyperfine Interact. **5**, 201 (1978).
[55] E.J.W. Verwey. Nature **144**, 327 (1939).
[56] T. Merceron, C. Djega-Mariadassou, J.L. Dormann, J. Magn. Magn. Mater. **31**–**34**, 781 (1983).

[57] B. Issa, I. Obaidat, B. Albiss, Y. Haik. Int. J. Mol. Sci. **14**, 21266 (2013) http://www.mdpi.com/1422-0067/14/11/21266.
[58] A.E. Berkowitz, W.J. Schuele, P.J. Flanders, J. Appl. Phys. **39**, 1261 (1968). DOI: 10.1103/physrevlett.27.1140.
[59] J.M.D. Coey. Phys. Rev. Lett **27**, *17*, 1140 (1971).
[60] S. Mørup, M.F. Hansen, C. Frandsen. Materials Science and Materials Engineering. Comprehensive Nanoscience and Nanotechnology. 2-d ed. Magn. Nanopart. **1**, 89 (2019). https://doi.org/10.1016/B978-0-12-803581-8.11338-4
[61] A.S. Kamzin, L.A. Grigoriev. Pis'ma v ZhETF **57**, 543 (1993). (in Russian). A.S. Kamzin, L.A. Grigoriev. ZhETF **104**, 3489 (1993). (in Russian).
[62] A.S. Kamzin, V.P. Rusakov, L.A. Grigoriev. Physics of Transition Metals. Int. Conf. USSR(1988). Proc. Pt. II. P. 271.
[63] A.S. Kamzin, L.A. Grigoriev, Pis'ma v ZhETF, **16**, *16*, 38 (1990), A.S. Kamzin, L.A. Grigoriev. ZhTF **60**, *7*, 151 (1990). (in Russian).
[64] F. Schaaf, U. Gonser. Hyperfine Interact. **57**, 2101 (1990). U. Gonzer, P. Schaaf, F. Aubertin. Hyperfine Interact. **66**, 95 (1991).
[65] A.S. Kamzin, L.P. Olkhovik, V.L. Rosenbaum. Pis'ma v ZhETF **61**, 916, (1995). (in Russian).
[66] L. Neel. J. Phys. Rad. **15**, *4*, 225 (1954).
[67] A.S. Kamzin, L.A. Grigor'ev. JETP Lett. **57**, *9*, 557 (1993).
[68] A.S. Kamzin. JETP **89**, *5*, 891 (1999).
[69] A.S. Kamzin, L.P. Ol'khovik, V.L. Rozenbaum. Phys. Solid State **41**, *3*, 433 (1999).
[70] A.S. Kamzin, V.L. Rozenbaum, L.P. Ol'khovik. JETP Lett. **67**, *10*, 843 (1998).
[71] A.S. Kamzin, L.P. Ol'khovik. Phys. Solid State **41**, *10*, 1658 (1999).
[72] A.S. Kamzin, I.M. Obaidat, A.A. Valiullin, V.G. Semenov, I.A. Al-Omari. Phys. Solid State **62**, *10*, 1933 (2020). DOI: https://link.springer.com/article/10.1134/S1063783420100157.
[73] M.E. Matsnev, V.S. Rusakov. AIP Conf. Proc. 1489, 178 (2012).
[74] G.N. Konygin, O.M. Nemtsova, V.E. Porsev. Zhurn. prikl. spektroskopii **86**, 374 (2019). (in Russian).
[75] M. Eibschuts, S. Shtrikman. J. Appl. Phys. **39**, 997 (1968).
[76] M.A. Chuev. J. Exp. Theor. Phys. **114**, 609 (2012). DOI: 10.1134/S1063776112020185.
[77] Dézsi, Cs. Fetzer, Á. Gombkötö, I. Szücs, J. Gubicza, T. Ungár. J. App. Phys. **103**, 104312 (2008). DOI: 10.1063/1.2937252
[78] M.A. Shipilin, I.N. Zakharova, A.M. Shipilin, V.I. Bachurin. Poverkhnost'. Rentgenovskie, sinkhrotronnye i neytronnye issledovaniya **6**, 45 (2014). (in Russian). DOI: 10.7868/S0207352814060171
[79] A.-F. Lehlooh, S.H. Mahmood. J. Magn. Magn. Mater. **151**, 163 (1995).
[80] H.Y. Hah, S. Gray, C.E. Johnson, J.A. Johnson, V. Kolesnichenko, P. Kucheryavy, G. Goloverda. J. Magn. Magn. Mater. **539**, 168382 (2021).
[81] V.V. Grecu, S. Constantinescu, M.N. Grecu, R. Olar, M. Badea, R. Turcu, Hyperfine Interact. **183**, 205 (2008).
[82] E. Umut. Hittite J. Sci. Eng. **6**, 243 (2019). DOI: 10.17350/HJSE19030000154.
[83] S.V. Bhandare, R. Kumar, A.V. Anupama, H.K. Choudhary, V.M. Jali, B. Sahoo. J. Magn. Magn. Mater. **433**, 29 (2017). http://dx.doi.org/10.1016/j.jmmm.2017.02.040.
[84] S.K. Shaw, J. Kailashiya, Santosh K. Gupta, C.L. Prajapat, Sher Singh Meena, D. Dash, P. Maiti, N.K. Prasad. J. Alloys Comp. **899**, 163192 (2022). https://doi.org/10.1016/j.jallcom.2021.163192.
[85] M. Popa, P. Bruna, D. Crespo, J.M.C. Moreno. J. Am. Ceram. Soc. **91**, 2488 (2008). DOI: 10.1111/j.1551-2916.2008.02501.x.
[86] W.H. Kwon, Jae-Gwang Lee, W.O. Choi, K.P. Chae. J. Magnet. **18**, 26 (2013). http://dx.doi.org/10.4283/JMAG.2013.18.1.026.
[87] M. Sorescu, D. Mihaila-Tarabasanu, L. Diamandescu. App. Phys. Let. **72**, 2047 (1998); DOI: 10.1063/1.121260.

Translated by A.Akhtyamov